

OTJR: Optimal Transport Meets Optimal Jacobian Regularization for Adversarial Robustness

Binh M. Le¹, Shahroz Tariq², Simon S. Woo¹

¹Sungkyunkwan University, South Korea

²CSIRO's Data61, Australia

bmle@g.skku.edu, shahroz.tariq@data61.csiro.au, swoo@g.skku.edu

Abstract

Deep neural networks are widely recognized as being vulnerable to adversarial perturbation. To overcome this challenge, developing a robust classifier is crucial. So far, two well-known defenses have been adopted to improve the learning of robust classifiers, namely adversarial training (AT) and Jacobian regularization. However, each approach behaves differently against adversarial perturbations. First, our work carefully analyzes and characterizes these two schools of approaches, both theoretically and empirically, to demonstrate how each approach impacts the robust learning of a classifier. Next, we propose our novel Optimal Transport with Jacobian regularization method, dubbed OTJR, jointly incorporating the input-output Jacobian regularization into the AT by leveraging the optimal transport theory. In particular, we employ the Sliced Wasserstein (SW) distance that can efficiently push the adversarial samples' representations closer to those of clean samples, regardless of the number of classes within the dataset. The SW distance provides the adversarial samples' movement directions, which are much more informative and powerful for the Jacobian regularization. Our extensive experiments demonstrate the effectiveness of our proposed method, which jointly incorporates Jacobian regularization into AT. Furthermore, we demonstrate that our proposed method consistently enhances the model's robustness with CIFAR-100 dataset under various adversarial attack settings, achieving up to 28.49% under AutoAttack.

1 Introduction

Deep Neural Networks (DNNs) have established themselves as the de facto method for tackling challenging real-world machine learning problems. Their applications cover a broad range of domains, such as image classification, object detection, and recommendation systems. Nevertheless, recent research has revealed DNNs' severe vulnerability to adversarial examples [Christian *et al.*, 2013; Ian *et al.*, 2014], particularly in computer vision tasks. Small imperceptible perturbations added to the image can easily deceive the neural

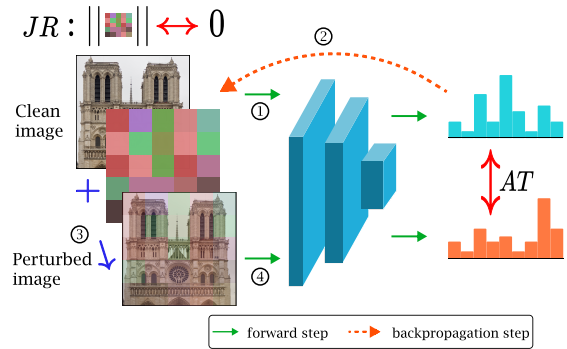


Figure 1: **Illustration of two popular approaches to boost a model's robustness: Adversarial Training (AT) vs. Jacobian regularization (JR).** The circled numbers indicate steps used in a typical AT framework. Jacobian regularization tries to silence the Jacobian matrix at the input end (after 2^{nd} step). The AT adjusts the distribution of perturbed samples at the output end (after 4^{th} step). For simplicity, we depict the backward step of Jacobian regularization and AT with the common dashed arrow. Jacobian regularization backpropagates through random projections, whereas the AT via a loss function. Our proposed OTJR integrates both, AT and Jacobian regularization, by the optimal transport theory.

networks into making incorrect predictions with high confidence. Moreover, this unanticipated phenomenon raises social concerns about DNNs' safety and trustworthiness, as they can be abused to attack many sophisticated and practical machine learning systems putting human lives into danger, such as in autonomous car [Deng *et al.*, 2020] or medical systems [Ma *et al.*, 2021; Bortsova *et al.*, 2021].

Meanwhile, there are numerous studies that devote their efforts to enhance the robustness of various models against adversarial examples. Among the existing defenses, adversarial training (AT) [Ian *et al.*, 2014; Madry *et al.*, 2018] and Jacobian regularization (JR) [Jakubovitz and Giryas, 2018; Hoffman *et al.*, 2019] are the two most predominant and popular defense approaches. In AT, small perturbations are added to a clean image in its neighbor of L_p norm ball to generate adversarial samples. Thus, an adversarially trained model can force itself to focus more on the most relevant image's pixels. On the other hand, the second approach, Jacobian regularization, mitigates the effect of the perturbation to the model's decision boundary by suppressing its gradients. However, AT and Jacobian regularization have not been directly compared

in both theoretical and empirical settings. In this work, we provide a side-by-side comparison of AT and Jacobian regularization to obtain a better and more concrete understanding of the adversarial robustness of DNN models. In particular, we present the novel approach of using both Jacobian regularization and AT for boosting the adversarial robustness of a model from different perspectives as described in 1.

In this work, we first theoretically revisit how AT and Jacobian regularization have been differently derived for providing the adversarial robustness of a defense model. Secondly, we conduct an extensive empirical analysis to demonstrate the distinct impacts of Jacobian regularization and AT on different layers of a defensive DNN. For AT, a plethora of studies have been proposed, presenting unique strategies to encourage the learning of robust classifiers. [Zhang *et al.*, 2020; Zhang *et al.*, 2019; Rony *et al.*, 2019; Kannan *et al.*, 2018; Madry *et al.*, 2018]. Among these approaches, Sinkhorn Adversarial Training (SAT) [Bouniot *et al.*, 2021] undertakes a similar approach with our method to minimize the distribution between clean and adversarial samples using optimal transport theory. However, the pillar of their algorithms mainly relies on the Sinkhorn algorithm [Cuturi, 2013] to utilize the space discretization property [Vialard, 2019]. Therefore, their approach has several limitations in terms of handling high-dimensional data [Meng *et al.*, 2019; Petrovich *et al.*, 2020]. Particularly, the Sinkhorn algorithm blurs the transport plan by adding an entropic penalty to ensure the optimization’s convexity. The entropic penalty encourages the randomness of the transportation map. However, in high-dimensional spaces, such randomness reduces the deterministic movement plan of one sample, causing ambiguity. As a result, when training defense models on a large scale dataset, SAT results in a slow convergence rate, which is unjustifiable due to the introduction of additional training epochs with distinct learning schedules [Pang *et al.*, 2020].

To this end, we introduce the novel Optimal Transport with Jacobian regularization OTJR method. We leverage the Sliced Wasserstein (SW) distance, which is more efficient for AT in high dimensional space with a faster convergence rate. In addition, the SW distance provides us with other advantages due to optimal movement directions of adversarial samples in the embedding space, which is critical for designing an effective defense. We further integrate the input-output Jacobian regularization by substituting its random projections with the optimal movements and constructing the optimal Jacobian regularization. Our main contributions are summarized as follows¹:

- **A Side-By-Side Theoretical and Empirical Comparison.** We first revisit the theory of adversarial robustness from the perspective of AT and Jacobian regularization. We are the first to analyze and provide a side-by-side comparison, and characterize the difference in impacts of each approach on a defensive DNN design.
- **Application of the Sliced Wasserstein (SW) Distance.** We propose the application of the SW distance in our

¹Our code is included in the *Supplementary Material*, and we plan to release the entire code upon acceptance of the paper.

AT Framework	Training Objective
TRADES	$\mathcal{L}_{\mathcal{X}\mathcal{E}}(\mathbb{S}(z), y) + \lambda \mathcal{L}_{\mathcal{X}\mathcal{E}}(\mathbb{S}(\tilde{z}), \mathbb{S}(z))$
PGD-AT	$\mathcal{L}_{\mathcal{X}\mathcal{E}}(\mathbb{S}(\tilde{z}), y)$
ALP	$\alpha \mathcal{L}_{\mathcal{X}\mathcal{E}}(\mathbb{S}(\tilde{z}), y) + (1 - \alpha) \mathcal{L}_{\mathcal{X}\mathcal{E}}(\mathbb{S}(\tilde{z}), y) + \lambda \ \tilde{z} - z\ _2$

Table 1: Training objectives of the popular AT frameworks, where \mathbb{S} denotes the softmax function.

AT, called OTJR, which can rapidly improve the convergence of the training procedure compared to prior works. With the support of SW, we derive **the optimal movement directions** of adversarial samples in the latent space. Then, we integrate these optimal directions into the Jacobian regularization, which can further increase the decision boundaries of DNNs.

- **White- and Black-box Attack Performance.** Through extensive experiments, we show that our proposed OTJR method achieves higher performance compared to the well-known SOTA defense mechanisms, demonstrating the effectiveness and competitiveness of optimizing Jacobian regularization in AT.

2 Comparisons between AT and JR

2.1 Theoretical Preliminaries

Let a function f represent a deep neural network (DNN), which is parameterized by θ , and $x \in \mathbb{R}^I$ be a clean input image. Its corresponding output vector is $z = f(x) \in \mathbb{R}^C$, where z_c is proportional to the likelihood that x is in the c -th class. Also, let $\tilde{x} = x + \epsilon$ be an adversarial sample of x generated by adding a small perturbation vector $\epsilon \in \mathbb{R}^I$. Then, the Taylor expansion of the mapped feature of the adversarial sample with respect to ϵ is derived as follows:

$$\begin{aligned} \tilde{z} &= f(x + \epsilon) = f(x) + J(x)\epsilon + O(\epsilon^2) \\ &\simeq z + J(x)\epsilon, \end{aligned} \quad (1)$$

$$\|\tilde{z} - z\|_q \simeq \|J(x)\epsilon\|_q. \quad (2)$$

Precisely, Eq. 2 is a basis to derive two primary schools of approaches, AT vs. Jacobian regularization, for mitigating adversarial perturbations and boosting the model robustness. In particular, each side of Eq. 2 targets the following two objectives, to improve the robustness:

1) Aligning adversarial representation (AT). Minimizing the left-hand side of Eq. 2 is to push the likelihood of an adversarial sample \tilde{x} close to that of a clean sample x . For instance, the Kullback-Leibler divergence between two likelihoods is a popular AT framework such as TRADES [Zhang *et al.*, 2019]. More broadly, the likelihood differences can include the cross-entropy ($\mathcal{X}\mathcal{E}$) loss of adversarial samples such as ALP [Kannan *et al.*, 2018], PGD-AT [Madry *et al.*, 2018], or FreeAT [Shafahi *et al.*, 2019]. These well-known AT frameworks are summarized in Table 1, to explain their core learning objective.

2) Regularizing input-output Jacobian matrix (JR). Regularizing the right-hand side of Eq. 2, which is indepen-

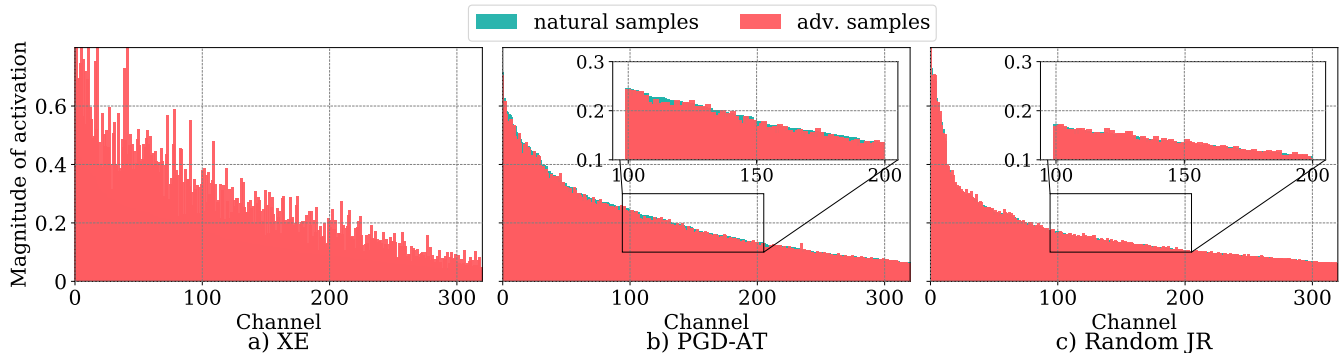


Figure 2: The magnitude of activation at the penultimate layer for models trained with $\mathcal{X}\mathcal{E}$ loss, PGD-AT adversarial training, and the input-output Jacobian regularization. The channels in the X-axis are sorted in descending order of the clean samples’ magnitude. More visualizations are provided in *Supp. Material*.

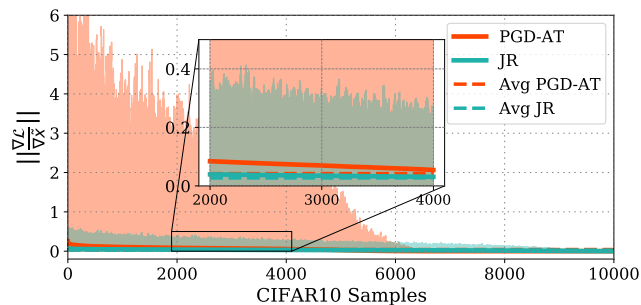


Figure 3: Magnitude of $\|\nabla_{\tilde{x}} \mathcal{L}_{\mathcal{X}\mathcal{E}}\|_1$ at the input layer for a model trained with PGD-AT and Jacobian regularization. Red and green-filled areas range from min. to max. values of each sample.

dent of \tilde{x} , suppresses the spectrum of the input-output Jacobian matrix $J(x)$. Thus, the model becomes more stable with respect to input perturbation, as it was theoretically and empirically demonstrated in a line of recent research [Jakubovitz and Giryes, 2018; Hoffman *et al.*, 2019; Co *et al.*, 2021]. Particularly, by observing $\|J(x)\epsilon\|_q \leq \|J(x)\|_F \|\epsilon\|$, one can instead minimize the square of the Frobenius norm of the Jacobian matrix, which can be estimated as follows [Hoffman *et al.*, 2019]:

$$\|J(x)\|_F^2 = C \mathbb{E}_{\hat{v} \sim \mathcal{S}^{C-1}} [\|\hat{v} \cdot J\|^2], \quad (3)$$

where \hat{v} is an uniform random vector drawn from a C -dimensional unit sphere \mathcal{S}^{C-1} . Using Monte Carlo method to approximate the integration of \hat{v} over the unit sphere, Eq. 3 can be rewritten as follows:

$$\|J(x)\|_F^2 = \frac{1}{n_{\text{proj}}} \sum_{i=1}^{n_{\text{proj}}} \left[\frac{\partial(\hat{v}_i \cdot z)}{\partial x} \right]^2. \quad (4)$$

Considering a large number of samples in a mini-batch, n_{proj} is usually set to 1 for the efficient computation. Hence, the Jacobian regularization is expressed as follows:

$$\|J(x)\|_F^2 \simeq \left[\frac{\partial(\hat{v} \cdot z)}{\partial x} \right]^2, \hat{v} \sim \mathcal{S}^{C-1}. \quad (5)$$

Summary. As shown above, each approach takes different direction to tackle adversarial perturbations. While AT tar-

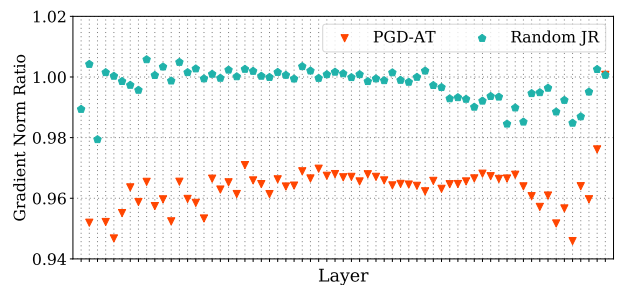


Figure 4: Ratios of $\mathbb{E}(\|\nabla_{\theta_i} \mathcal{L}(\tilde{x})\| / \|\nabla_{\theta_i} \mathcal{L}(x)\|)$ w.r.t. the model’s parameters θ_i on CIFAR-10. The lower the ratios are, the more emphasis the model puts on perturbations.

gets aligning the likelihoods at the output end, Jacobian regularization tries to force the norm of the Jacobian matrix at the input to zero, as also pictorially described in Fig. 1. However, their distinct effects on the robustness of a DNN have not been fully compared and analyzed so far.

2.2 Empirical Analysis

We also conduct an experimental analysis to ascertain and characterize the distinct effects of the two approaches (AT vs. Jacobian regularization) on a defense DNN when it is trained with each of the objectives. We use wide residual network WRN34 as the preliminary baseline architecture on CIFAR-10 dataset and apply two canonical frameworks: PGD-AT [Madry *et al.*, 2018] and input-output Jacobian regularization [Hoffman *et al.*, 2019] to enhance the model’s robustness. Details of training settings are provided in the experiment section.

In particular, we measure the magnitude of channel-wise activation to characterize the connection between adversarial defense methods and the intermediate layer’s activation [Bai *et al.*, 2021]. Fig. 2 provides the average magnitude of penultimate activation of clean vs. adversarial samples created by PGD-20 attacks [Madry *et al.*, 2018]. As shown in Fig. 2, not only AT [Bai *et al.*, 2021], but also Jacobian regularization can effectively suppress the magnitude of the activation. Moreover, the Jacobian regularization typically achieves the

lower magnitude value of the activation compared to that of PGD-AT. This observation serves as a clear counter-example to earlier results from Bai *et al.*, where they claim that adversarial robustness can be generally achieved via channel-wise activation suppressing. As such, it is worth noting that while a more effective defense strategy can produce lower activation, the inverse is not always true. In addition, Fig. 3 represents the average gradient of $\mathcal{X}\mathcal{E}$ loss with respect to the adversarial samples, at the input layer. This demonstrates that the model trained with Jacobian regularization suppresses input gradients more effectively than a typical AT framework, *i.e.*, PGD-AT. In other words, when a defensive model is abused to generate adversarial samples, pre-training with Jacobian regularization can reduce the severity of perturbations, hindering the adversary’s target.

On a layer-by-layer basis, we provide Fig. 4 to depict the gradients of models trained with PGD-AT, and Jacobian regularization, respectively. Particularly, we compute the norm ratios of the loss gradient on the adversarial sample to the loss gradient on the clean samples for each layer of the model. As we can observe, the model trained with the Jacobian regularization produces higher ratio values, meaning it puts less emphasis on adversarial samples due to its agnostic defense mechanism. Meanwhile, most of the ratio values at the middle layers from Jacobian training vary around 1. This is explained by the regularization applied to its first derivatives. In summary, we can also empirically conclude that the Jacobian regularization tends to silence the gradient of the model from output to input layers. Therefore, it *agnostically* stabilizes the model under the changes of input samples, and produces low-magnitude adversarial perturbations, when the model is attacked. In contrast, by learning the meaningful pixels from input images, AT adjusts the model’s parameters at every layer in such a way to reduce the impacts of adversarial perturbation on the model’s outputs.

As demonstrated by Hoffman *et al.*, the increase of computational cost from a model training with Jacobian regularization is insignificant, compared to standard training. Therefore, a combination of AT and Jacobian regularization becomes an appealing approach for the adversarial robustness of a model. Furthermore, taking advantages from both approaches can effectively render a classifier to suppress the perturbation and adaptively learn crucial features from both clean and adversarial samples. However, merely adding both approaches together into the training loss is not the best option. Indeed it is insufficient, since the adversarial representations in the latent space can contain meaningful information for the Jacobian regularization, which we will discuss more in the next section.

Therefore, in this work, we propose a novel optimization framework, OTJR, to leverage the movement direction information of adversarial samples in the latent space and optimize the Jacobian regularization. In this fashion, we can successfully establish a relationship and balance between silencing input’s gradients and aligning output distributions, and significantly improve the overall model’s robustness. In addition, recent studies have proposed approaches utilizing a surrogate model [Wu *et al.*, 2020] or teacher-student framework [Cui *et al.*, 2021] during training. Yet, while these methods improve

Algorithm 1 OTJR: AT with SW and optimal Jacobian regularization.

Require: DNN f parameterized by θ , training dataset \mathcal{D} . Number of projections K . Maximum perturbation ϵ , step size η , number of adversarial iteration P . Loss’ hyper-parameters λ_J and λ_{SW} . Learning rate α and batch size of \mathcal{B} .

while not converged **do**
 for $\{(x_i, y_i)\}_{\mathcal{B}} \in \mathcal{D}$ **do**
 $\nu := \{z_i\}_{\mathcal{B}} = f(x_i; \theta)|_{i=1, \dots, \mathcal{B}}$
 # Generate adv. samples
 for iteration $t \leftarrow 1$ to P **do**
 $\tilde{x}_i = \Pi_x^\epsilon(\tilde{x}_i + \eta \cdot \text{sgn}(\nabla_{\tilde{x}_i} \mathcal{L}(\tilde{x}_i, y_i)))|_{i=1, \dots, \mathcal{B}}$
 end for
 $\mu := \{\tilde{z}_i\}_{\mathcal{B}} = f(\tilde{x}_i; \theta)|_{i=1, \dots, \mathcal{B}}$
 $SW \leftarrow 0$
 $\Delta_i \leftarrow 0|_{i=1, \dots, \mathcal{B}}$
 for iteration $k \leftarrow 1$ to K **do**
 # Sample \hat{v}_k from \mathcal{S}^{C-1}
 $\hat{v}_k \leftarrow \mathcal{U}(\mathcal{S}^{C-1})$
 # Add SW under projection \hat{v}_k
 $SW \leftarrow SW + \psi(\tau_1 \circ \mathcal{R}_{\hat{v}_k} \mu, \tau_2 \circ \mathcal{R}_{\hat{v}_k} \nu)$
 # Calculate samples’ movements
 under \hat{v}_k
 $m_k \leftarrow (\tau_1^{-1} \circ \tau_2 \circ \mathcal{R}_{\hat{v}_k} \nu - \mathcal{R}_{\hat{v}_k} \mu) \otimes \hat{v}_k$
 $\Delta_i \leftarrow \Delta_i + m_{k,i}|_{i=1, \dots, \mathcal{B}}$
 end for
 $\Delta_i \leftarrow \Delta_i / \|\Delta_i\|_2 |_{i=1, \dots, \mathcal{B}}$
 $\mathcal{L} \leftarrow \sum^{\mathcal{B}} (\mathcal{L}_{\mathcal{X}\mathcal{E}}(\tilde{x}_i, y_i) + \lambda_J \|J(x_i | \Delta_i)\|_F^2)$
 + $\lambda_{SW} SW(\mu, \nu)$
 $\theta \leftarrow \theta - \alpha \cdot \nabla_{\theta} \mathcal{L}$
 end for
end while

the model’s robustness, they also rely on previous training losses (such as TRADE or PGD). And they introduce additional computation for the AT, which are so far well-known for their slow training speed and computational overhead. In our experiment, we show that our novel training loss can be compatible with these frameworks and further improve the model’s robustness by a significant margin compared to prior losses.

3 Our Approach

Our approach explores the Sliced Wasserstein (SW) distance in order to push the adversarial distribution closer to the natural distribution with a faster convergence rate. Next, we propose optimal movement directions obtained from the SW distance to sufficiently minimize the spectrum of input-output Jacobian matrix.

Sliced Wasserstein distance. The p -Wasserstein distance between two probability distributions μ and ν [Villani, 2008] in the d -dimensional space Ω , to search for an optimal transportation cost between μ and ν , is defined as follows:

$$W_p(P_\mu, P_\nu) = \left(\inf_{\pi \in \Pi(\mu, \nu)} \int_{\Omega \times \Omega} \psi(x, y)^p d\pi(x, y) \right)^{1/p}, \quad (6)$$

where $\phi : \Omega \times \Omega \rightarrow \mathbb{R}^+$ is a transportation cost function, and $\Pi(\mu, \nu)$ is a collection of all possible transportation plans. The Sliced p -Wasserstein distance (SW_p), which is inspired by the W_p in one-dimensional, calculates the p -Wasserstein distance by projecting μ and ν onto multiple one-dimensional marginal distributions using Radon transform [Helgason, 2010]. The SW_p is defined as follows:

$$SW_p(\mu, \nu) = \int_{S^{d-1}} W_p(\mathcal{R}_{\hat{v}}\mu, \mathcal{R}_{\hat{v}}\nu) d\hat{v}, \quad (7)$$

where $\mathcal{R}_{\hat{v}}\mu$ is the Radon transform as follows:

$$\mathcal{R}_{\hat{v}}\mu = \int_{\Omega} \mu(x) \delta(t - \langle \hat{v}, x \rangle) dx, \forall t \in \mathbb{R}, \quad (8)$$

where $\langle \cdot, \cdot \rangle$ denote the Euclidean inner product, and δ is the Dirac delta function.

Next, let \mathcal{B} denote the size of a mini-batch of samples. To calculate the transportation cost between adversarial samples' representations $\mu := \{\tilde{z}_i\}_{\mathcal{B}}$ and the corresponding original samples' representations $\nu := \{z_i\}_{\mathcal{B}}$, the integration of \hat{v} over the unit sphere S^{C-1} is approximated via Monte Carlo method with K uniformly sampled random vector $\hat{v}_i \in S^{C-1}$. In particular, $\mathcal{R}_{\hat{v}_i}\mu$ and $\mathcal{R}_{\hat{v}_i}\nu$ are sorted in ascending order using two permutation operators τ_1 and τ_2 , respectively, and the approximation of Sliced l -Wasserstein is expressed as follows:

$$SW(\mu, \nu) \simeq \sum_{k=1}^K \psi(\tau_1 \circ \mathcal{R}_{\hat{v}_k}\mu, \tau_2 \circ \mathcal{R}_{\hat{v}_k}\nu). \quad (9)$$

Optimal movement direction. Using Eq. 9, we can straightforwardly compute the trajectory of each \tilde{z}_i in the latent space \mathbb{R}^C in order to minimize the $SW(\mu, \nu)$. We refer to the directions of these trajectories as *optimal movement directions*, because the SW distance produces the lowest transportation cost between the source and target distributions. Particularly, let the trajectories of $\{\tilde{z}_i\}_{\mathcal{B}}$ in each single projection \hat{v}_k be:

$$m_k = (\tau_1^{-1} \circ \tau_2 \circ \mathcal{R}_{\hat{v}_k}\nu - \mathcal{R}_{\hat{v}_k}\mu) \otimes \hat{v}_k, \quad (10)$$

where \otimes denotes the outer product. Then, the overall optimal movement direction of each \tilde{z}_i is expressed as follows:

$$\Delta_i = \frac{\sum_{k=1}^K m_{k,i}}{\|\sum_{k=1}^K m_{k,i}\|_2}. \quad (11)$$

For illustration, we present a toy example of optimal movement directions obtained by Eq. 11 in Fig. 5. The movement direction of an adversarial sample \tilde{x} in the latent space indicates the most sensitive direction of x under adversarial perturbations. Therefore, we aim to regularize the Jacobian matrix of x under this optimal direction, in contrast to a random projection as was proposed in [Hoffman *et al.*, 2019]. Using Eq. 5, we can rewrite the optimal input-output Jacobian regularization with previously obtained informative projections for a sample as follows:

$$\|J(x_i|\Delta_i)\|_F^2 \simeq \left[\frac{\partial(\Delta_i \cdot z_i)}{\partial x_i} \right]^2. \quad (12)$$

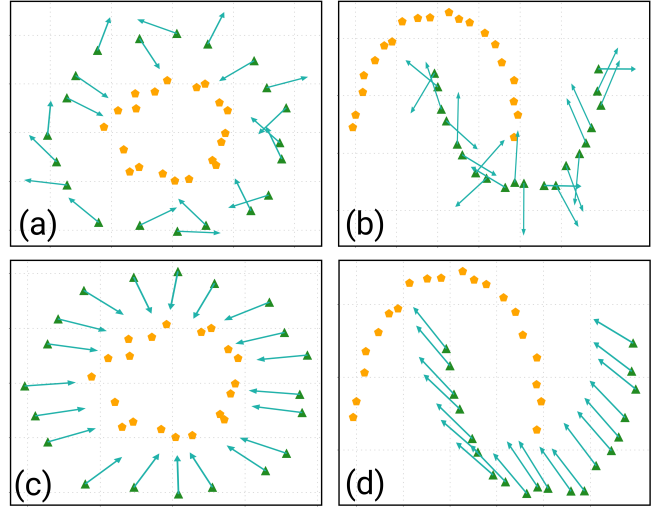


Figure 5: Illustration of optimal movement directions. **Top row** ((a) & (b)): Random movement directions (green arrows), which is non-informative, uniformly sampled from two-dimensional unit sphere S^1 . **Bottom row** ((c) & (d)): The optimal movement directions from the SW distance between source distribution (green) and target distribution (orange) obtained from Eq. 11.

Then, our overall loss function for a batch of samples $\{(x_i, y_i)\}_{\mathcal{B}}$ is expressed in the following way:

$$\mathcal{L} = \sum_{i=1}^{\mathcal{B}} (\mathcal{L}_{\mathcal{X}\mathcal{E}}(\tilde{x}_i, y_i) + \lambda_J \|J(x_i|\Delta_i)\|_F^2) + \lambda_{SW} SW(\mu, \nu). \quad (13)$$

In practice, sampling K uniform vectors \hat{v}_k can be performed simultaneously thanks to deep learning libraries. Then, the calculation of random projections and optimal movement steps can be vectorized. Our end-to-end algorithm for optimizing Eq. 13 is provided in Algorithm 1 and List 1 (*Supp. Material*).

4 Experimental Results

4.1 Experiment Settings

We employ WideResNet34-10 [Zagoruyko and Komodakis, 2016] as our backbone architecture on two datasets CIFAR-10 and CIFAR-100 [Krizhevsky *et al.*, 2009]. The model are trained for 100 epochs with the momentum SGD [Qian, 1999] optimizer, whereas its initial learning rate is set to 0.1 and decayed by a factor of 10 at 75th and 90th epoch, respectively. Adversarial samples in the training phase are generated by L_∞ -PGD [Madry *et al.*, 2018] in 10 iterations with the maximal perturbation $\epsilon = 8/255$ and the perturbation step size $\eta = 2/255$. For a fair comparison with different approaches [Pang *et al.*, 2020], we use the above settings throughout our experiments without early stopping or modifying models' architecture, and report their performances on the last epoch. For our OTJR based defense models, we use the following hyper-parameter settings: $\{K = 32, \lambda_J = 0.002, \lambda_{SW} = 64\}$ and $\{K = 128, \lambda_J = 0.001, \lambda_{SW} = 64\}$ for CIFAR-10 and CIFAR-100, respectively. An ablation study of the

Dataset	Defense	Clean	PGD ²⁰	PGD ¹⁰⁰	L_2 -PGD	MIM	FGSM	CW	FAB	Square	SimBa	AutoAtt
CIFAR-10	TRADES	84.65	54.33	54.06	61.23	54.27	60.59	53.44	54.20	62.50	71.29	52.26
	ALP	86.77	47.31	46.72	56.15	47.12	58.42	47.80	55.37	59.64	68.71	46.55
	PGD-AT	86.74	46.75	46.26	55.91	46.66	56.53	47.49	48.39	59.01	68.58	45.81
	SAT	82.96	53.60	53.34	60.44	50.58	60.36	52.38	53.05	61.66	69.90	50.99
	Random JR	85.18	22.63	21.91	60.71	22.40	32.90	21.95	21.85	46.14	70.92	20.38
	SW	84.77	54.11	53.78	61.24	54.19	61.48	53.84	55.30	63.11	71.02	51.89
	OTJR (Ours)	84.53	55.07	54.69	63.99	55.03	61.09	53.92	54.26	63.27	72.79	52.41
CIFAR-100	TRADES	57.61	30.46	30.46	35.92	30.43	33.16	28.14	27.86	33.75	44.47	27.13
	ALP	60.60	26.10	25.75	33.66	26.08	31.51	25.60	25.70	32.91	43.17	24.49
	PGD-AT	60.05	24.07	23.78	31.56	23.97	29.45	24.68	24.55	31.51	41.30	23.27
	SAT ₄₀₀	54.34	26.82	26.64	32.36	26.84	31.24	25.30	26.69	31.35	40.57	24.38
	Random JR	66.64	9.54	8.99	37.98	9.42	16.58	10.40	9.28	23.32	49.48	7.98
	SW	58.06	26.22	26.15	31.56	26.18	31.11	25.78	26.20	31.61	41.24	24.70
	OTJR (Ours)	58.14	32.41	32.26	43.30	32.34	34.68	29.65	29.30	36.34	50.07	28.49

Table 2: **Classification accuracy (%) under white-box, black-box attacks and AutoAttack.** Different defense methods trained on CIFAR-10 and CIFAR-100 datasets using WRN34 in 100 epochs, where underscript indicates training epochs. Best results are in **bold**.

hyper-parameters’ impact on model performance is provided in *Supp. Material*. In addition, we perform the basic sanity tests [Carlini *et al.*, 2019] in *Supp. Material* to ensure that our proposed OTJR does not rely on gradient obfuscation. Overall, we compare our method with four different recent SOTA AT frameworks: TRADES [Zhang *et al.*, 2019], ALP [Kannan *et al.*, 2018], PGD-AT [Madry *et al.*, 2018], and SAT [Bouniot *et al.*, 2021]. The experiments are conducted on one GeForce RTX 3090 24GB GPU with Intel Xeon Gold 6230R CPU @ 2.10GHz.

4.2 Adversarial Attacks

Follow Zhang *et al.*, we evaluate defense methods under a wide range *white-box* attacks (20 iterations)²: FGSM [Ian *et al.*, 2014], PGD [Madry *et al.*, 2018], MIM [Dong *et al.*, 2018], CW_∞ [Carlini and Wagner, 2017], DeepFool [Moosavi-Dezfooli *et al.*, 2016], and FAB [Croce and Hein, 2020a]; and a *black-box* attacks (1000 iterations): Square [Andriushchenko *et al.*, 2020]. We use the same parameters as Rice *et al.* for our experiments: for the $L_∞$ threat model, the values of epsilon and step size are 8/255 and 2/255 for CIFAR-10 and CIFAR-100, respectively. For the L_2 threat model, the values of epsilon and step size are 128/255 and 15/255 for all datasets. Additionally, we include AutoAttack [Croce and Hein, 2020b] which is a reliable adversarial evaluation framework and an ensemble of four diverse attacks: APGD-CE, APGD-DLR [Croce and Hein, 2020b], FAB [Croce and Hein, 2020a], and Square [Andriushchenko *et al.*, 2020]. The results of this experiment are presented in Table 2, where the best results are highlighted in bold. As shown, our proposed OTJR method demonstrates its superior performance across different attack methods. The improvement is considerable, by more than 1.0% and 2.3% on average compared to other methods on CIFAR-10 and CIFAR-100, respectively. In addition, we include two primary components of our proposed OTJR, *i.e.*, SW and random JR in Table 2. While the random JR, as expected, is highly vulnerable to

²<https://github.com/Harry24k/adversarial-attacks-pytorch.git>

Loss	AWP		LBGAT	
	Clean	AutoAtt	Clean	AutoAtt
TRADES	60.17	28.80	60.43	29.34
OTJR	60.55	29.79	62.15	29.64

Table 3: Classification accuracy (%) from defense losses integrated AWP and LBGAT. Best results are in **bold**.

Defense	Clean	MIM	CW	Square	AutoAtt
	IMAGENET100 - PreActResNet18				
TRADES	62.64	30.66	56.95	46.52	24.86
SAT ⁴⁰⁰	45.08	29.08	41.56	36.14	23.96
OTJR	61.97	33.20	57.42	49.00	27.54
INTEL- ResNet50					
TRADES	54.43	3.73	2.47	5.57	0.07
SAT	50.17	5.93	4.73	6.77	1.60
OTJR	57.80	8.27	6.77	9.37	3.74

Table 4: Classification accuracy (%) of PreActResNet18 and ResNet50 with IMAGENET100 and INTEL dataset, respectively, under *white-* and *black-box* attacks. Best results are in **bold**.

most of the *white-box* attacks due to its adversarial-agnostic defense strategy, the SW approach is on par with other AT methods.

4.3 Compatibility with different frameworks and datasets.

Frameworks with surrogate models. AWP [Wu *et al.*, 2020] and LBGAT [Cui *et al.*, 2021] are two SOTA benchmarks boosting adversarial robustness using surrogate models during training, albeit rather computationally expensive. Furthermore, they utilized existing AT losses, such as TRADES. We integrate our proposed optimization loss into AWP and LBGAT, respectively, and present its performance at the *final training epoch*. We selected TRADES as the best existing loss function that was deployed with these frameworks and experimented with CIFAR-100-WRN34 for comparison.

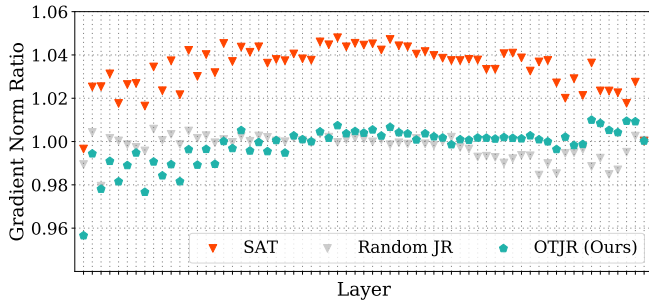


Figure 6: **Average gradient norm ratios between adversarial and clean samples.** The ratios of $\mathbb{E}(\|\nabla_{\theta_i} \mathcal{L}(\hat{x})\| / \|\nabla_{\theta_i} \mathcal{L}(x)\|)$ with respect to the model’s parameters θ_i on CIFAR-10 dataset.

Method	$\mathbb{E}(\ \nabla_x \mathcal{L}\ _1)$	Method	$\mathbb{E}(\ \nabla_x \mathcal{L}\ _1)$
$\mathcal{X}\mathcal{E}$	$854e^{-4}$	PGD-AT	$158e^{-4}$
ALP	$118e^{-4}$	TRADES	$45e^{-4}$
SAT	$48e^{-4}$	OTJR (<i>Ours</i>)	$43e^{-4}$

Table 5: **Average derivative of $\mathcal{X}\mathcal{E}$ loss *w.r.t.* input x at the pixel level.** The lower the derivative is, the less perturbed the adversarial samples are when the model is abused. Best results are in **bold**.

As shown in Table 3, our OTJR is compatible with the two frameworks and surpasses the baseline performance by a significant margin.

High-quality datasets with different backbones. We further explore the robustness of the models trained with our OTJR and the two most competitive AT frameworks, namely TRADES and SAT, on high quality datasets. Particularly, we experiment on IMAGENET100 [Deng *et al.*, 2009], and INTEL image dataset [Bansal, 2019], using PreActResNet18 [He *et al.*, 2016b] and ResNet50 [He *et al.*, 2016a], respectively. For INTEL dataset, the hyper-parameter settings are kept the same as for CIFAR-10 dataset, except that the learning rate is $1e^{-3}$ decayed by 0.1 every 7 epochs, and the model is trained in 50 epochs. Meanwhile, IMAGENET100 is trained with the same settings as CIFAR-100, except that SAT is trained in 400 epochs. In Table 4, we report the results with strongest attacks from Table 2, MIM, CW (*white-box*) Square attack (*black-box*), and AutoAttack. Under our defense framework, our model achieves much higher robustness than others, while maintaining comparative accuracy on clean images. The results demonstrate that our OTJR is compatible to various backbone networks as well as different classification tasks.

4.4 Ablation Studies & Discussion

Loss’s derivative. Similar to the preliminary experiment, we describe the differences between our proposed OTJR and SAT in terms of the defense model’s gradients at different layers. Throughout intermediate layers in an attacked model, both frameworks provide stable ratios between perturbed and clean sample’s gradients as shown in Fig. 6. It is worth noting that the gradients are derived on unobserved samples in the test set. As shown, in the forward path, our proposed OTJR

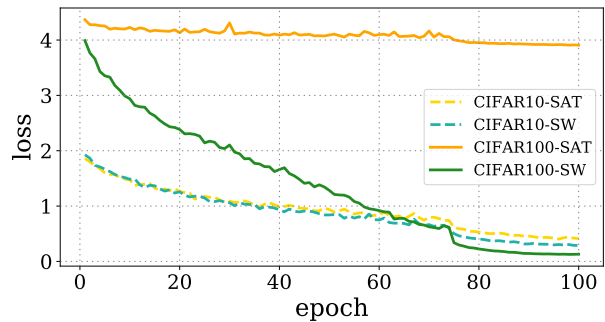


Figure 7: The $\mathcal{X}\mathcal{E}$ loss of WRN34 training on CIFAR-10 and CIFAR-100 with SW, and SAT, respectively. While both algorithms exhibit a similar convergence on CIFAR-10, SAT fails to converge on CIFAR-100 in 100 epochs.

successfully balances the adversarial samples and the clean samples, with ratio values in the majority of layers near to 1. Moreover, in the backward path, since the victim model’s gradients are deployed to generate more perturbations, our OTJR model achieves better robustness when it can produce smaller gradients *w.r.t.* its inputs.

Next, Table 5 shows the average magnitude of cross-entropy loss’s derivative *w.r.t.* the input images from CIFAR-10 dataset with WRN34. While all the AT methods can significantly reduce the impact of the gradient compared to $\mathcal{X}\mathcal{E}$ loss, our proposed framework introduces the lowest value at $43e^{-4}$. This finding explains why the OTJR successfully ensures enhanced resilience against the same adversary.

SW distance vs. Sinkhorn divergence. Bouniot *et al.* propose the SAT algorithm that deploys Sinkhorn divergence to push the distributions of clean and perturbed samples towards each other [Bouniot *et al.*, 2021]. While SAT can achieve comparable results to previous research, it exposes a weakness in high-dimensional space, i.e., datasets with a large number of classes exhibit slower convergence, as demonstrated in other research [Meng *et al.*, 2019; Petrovich *et al.*, 2020]. We also show that SAT fails to converge on CIFAR-100 in 100 epochs in our experiment, as shown in Fig. 7. Meanwhile, we observed that hyper-parameter settings highly affect the adversarial training [Pang *et al.*, 2020], and the performance improvement by SAT can be partly achieved with additional training epochs. Nevertheless, we still include results from SAT trained in 400 epochs on CIFAR-100 in [Bouniot *et al.*, 2021].

Our OTJR vs. Naive Combination of SAT & random JR. In order to reveal the contribution of the Jacobian regularization and how the naive approach (SAT+JR) differs from ours, we report their robustness under wide range of *white-box* PGD attack in Table 6. The experiments are conducted with CIFAR-10 and CIFAR-100 with WRN34. Our optimal approach attains slightly better robustness on small dataset (CIFAR-10). On the large dataset (CIFAR-100), however, our OTJR achieves significant improvement. This phenomenon is explained by the fact that regularizing the input-output Jacobian matrix increases the difficulty of the SAT algorithm’s convergence, which results in a slower convergence. Therefore, naively combining AT and random Jacobian regulariza-

Dataset	Defense	Clean	PGD ²⁰	PGD ¹⁰⁰	L ₂ -PGD	MIM	FGSM	CW	FAB	Square	SimBa	AutoAtt
CIFAR-10	SAT+JR	84.43	54.31	53.95	62.82	54.30	60.55	52.66	53.36	62.27	91.94	51.66
	OTJR (<i>Ours</i>)	84.53	55.07	54.69	63.99	55.03	61.09	53.92	54.26	63.27	72.79	52.41
CIFAR-100	SAT+JR ₄₀₀	53.77	26.07	25.83	33.06	26.04	30.69	24.89	26.21	31.16	40.93	24.10
	OTJR (<i>Ours</i>)	58.14	32.41	32.26	43.30	32.34	34.68	29.65	29.30	36.34	50.07	28.49

Table 6: Comparison between ours and SAT+Random JR on CIFAR-10 and CIFAR-100 with WRN34. Best results are in **bold**.

Dataset	Defense	Clean	PGD ²⁰	PGD ¹⁰⁰	L ₂ -PGD	MIM	FGSM	CW	FAB	Square	SimBa	AutoAtt
CIFAR-10	Random JR	85.18	22.63	21.91	60.71	22.40	32.90	21.95	21.85	46.14	70.92	20.38
	Optimal JR	84.42	25.39	24.62	62.27	25.22	34.74	24.63	24.54	46.98	71.99	22.90
CIFAR-100	Random JR	66.64	9.54	8.99	37.98	9.42	16.58	10.40	9.28	23.32	49.48	7.98
	Optimal JR	64.85	11.20	10.57	38.91	11.08	17.59	11.68	10.58	24.67	50.46	24.14

Table 7: Accuracy (%) of WRN34 model trained with JR having random projections, and informative projections respectively, under different number attacks on CIFAR-10 test dataset. Best results are in **bold**.

tion can restrain the overall optimization process.

Optimal vs. random projections. To verify the efficiency of the optimal Jacobian regularization, WRN34 is trained on CIFAR-10 using $\mathcal{X}\mathcal{E}$ loss with clean samples and the regularization term using Eq. 5 and Eq. 12 respectively, as follow:

$$\mathcal{L} = \sum_{i=1}^B (\mathcal{L}_{\mathcal{X}\mathcal{E}}(x_i, y_i) + \lambda_J \|J(x_i)\|_F^2), \quad (14)$$

where λ_J is a hyper-parameter to balance the regularization term and $\mathcal{X}\mathcal{E}$ loss that is set to 0.02 for this experiment. As we can observe from Table 7, the Jacobian regularized model trained with SW-supported projections consistently achieves higher robustness, compared to the random projections. As shown, our proposed optimal regularization consistently achieves up to 2.5% improvement in accuracy under *AutoAttack* compared to the random one.

In addition, we describe the benefits of the optimal Jacobian regularization in Fig. 9 (*Supp. Material*). While the model trained without the regularizer is highly vulnerable to the perturbation, the Jacobian regularizer can enhance its robustness by extending the decision boundaries, which is indicated by a larger black circle. Our optimal Jacobian regularizer can further expand the decision cell, thus additionally improving the model robustness. This is explained by the informative directions, as illustrated in Fig. 5, which can guide our model to achieve optimal projections for the input-output Jacobian regularization.

Hyper-parameter sensitivity Our ablation studies about hyper-parameters’ sensitivities, *i.e.*, λ_J , λ_{SW} and K , are included in Table 8. The experiments are conducted on CIFAR-10 with WRN34. First, we note that increasing λ_J too much may decrease both accuracy and robustness. The reason comes from the fact that the gradients of the loss function creates adversarial perturbations in AT step. Next, the values of λ_{SW} can be selected from a wide range. Nevertheless, a trained model with small λ_{SW} cannot force its parameters to pay more attention to adversarial samples, and a large λ_{SW} can decrease the original accuracy. Regarding the number of slices K , we note that a small number of slices can not

Hyper-parameters			Robustness			
λ_J	λ_{SW}	K	Clean	PGD ²⁰	PGD ¹⁰⁰	AutoAttack
0.002	64	32	84.53	55.07	54.69	52.41
0.01	64	32	84.75	54.37	54.06	52.13
0.05	64	32	82.82	54.98	54.72	52.00
0.002	32	32	85.47	54.85	54.46	52.23
0.002	72	32	83.19	55.70	55.40	53.04
0.002	64	16	81.47	55.10	54.98	51.82
0.002	64	64	85.79	53.80	53.36	51.83

Table 8: **Hyper-parameter tuning.** The sensitivities of hyper-parameters: λ_J , λ_{SW} and K . Without Jacobian regularization, the model cannot achieve the best performance. Trade-off between model’s accuracy vs. robustness is shown using different λ_{SW} . Default setting is **highlighted**.

generalize the transportation cost between the distributions in the latent space, while a very large K does not provide significant improvement, but can decelerate the training process. Finally, it is worth mentioning that there is still room for hyper-parameter tuning to achieve better results.

5 Conclusion

We first theoretically and empirically analyze the impacts of AT and Jacobian regularization on the robustness of DNN models. We show that the AT pays more attention to meaningful input samples’ pixels, whereas the Jacobian regularizer agnostically silences the DNN’s gradients under any perturbation from its output to input layers. Based on these characterizations, we effectively augment the AT framework by integrating input-output Jacobian matrix in order to more effectively improve the DNN’s robustness. Using the optimal transport theory, our work is the first to jointly minimize the difference between the distributions of original and adversarial samples with much faster convergence. Also, the proposed SW distance produces the optimal projections for the Jacobian regularization, which can further increase the deci-

sion boundaries of a sample under perturbations, and achieves much higher performance through optimizing the best of both worlds.

References

- [Andriushchenko *et al.*, 2020] Maksym Andriushchenko, Francesco Croce, Nicolas Flammarion, and Matthias Hein. Square attack: a query-efficient black-box adversarial attack via random search. In *European Conference on Computer Vision (ECCV)*, pages 484–501. Springer, 2020.
- [Athalye *et al.*, 2018] Anish Athalye, Nicholas Carlini, and David Wagner. Obfuscated gradients give a false sense of security: Circumventing defenses to adversarial examples. In *International conference on machine learning*, pages 274–283. PMLR, 2018.
- [Bai *et al.*, 2021] Yang Bai, Yuyuan Zeng, Yong Jiang, Shu-Tao Xia, Xingjun Ma, and Yisen Wang. Improving adversarial robustness via channel-wise activation suppressing. *International Conference on Learning Representations (ICLR)*, 2021.
- [Bansal, 2019] Puneet Bansal. Intel image classification - kaggle. <https://www.kaggle.com/puneet6060/intel-image-classification>, January 2019. [Online; accessed 17-November-2021].
- [Bortsova *et al.*, 2021] Gerda Bortsova, Cristina Gonzalez-Gonzalo, Suzanne Wetstein, Florian Dubost, Ioannis Karamados, Laurens Hogeweg, Bart Liefers, Bram Ginneken, Josien Pluim, Mitko Veta, et al. Adversarial attack vulnerability of medical image analysis systems: Unexplored factors. *Medical Image Analysis*, page 102141, 2021.
- [Bouniot *et al.*, 2021] Quentin Bouniot, Romaric Audigier, and Angélique Loesch. Optimal transport as a defense against adversarial attacks. In *2020 25th International Conference on Pattern Recognition (ICPR)*, pages 5044–5051. IEEE, 2021.
- [Carlini and Wagner, 2017] Nicholas Carlini and David Wagner. Towards evaluating the robustness of neural networks. In *2017 IEEE Symposium on Security and Privacy (SP)*, pages 39–57. IEEE, 2017.
- [Carlini *et al.*, 2019] Nicholas Carlini, Anish Athalye, Nicolas Papernot, Wieland Brendel, Jonas Rauber, Dimitris Tsipras, Ian Goodfellow, Aleksander Madry, and Alexey Kurakin. On evaluating adversarial robustness. *arXiv preprint arXiv:1902.06705*, 2019.
- [Christian *et al.*, 2013] Szegedy Christian, Zaremba Wojciech, Sutskever Ilya, Bruna Joan, Erhan Dumitru, Goodfellow Ian, and Fergus Rob. Intriguing properties of neural networks. *arXiv preprint arXiv:1312.6199*, 2013.
- [Co *et al.*, 2021] Kenneth T Co, David Martinez Rego, and Emil C Lupu. Jacobian regularization for mitigating universal adversarial perturbations. *30th International Conference on Artificial Neural Networks (ICANN)*, 2021.
- [Croce and Hein, 2020a] Francesco Croce and Matthias Hein. Minimally distorted adversarial examples with a fast adaptive boundary attack. In *International Conference on Machine Learning (ICML)*, pages 2196–2205. PMLR, 2020.
- [Croce and Hein, 2020b] Francesco Croce and Matthias Hein. Reliable evaluation of adversarial robustness with an ensemble of diverse parameter-free attacks. In *International conference on machine learning*, pages 2206–2216. PMLR, 2020.
- [Cui *et al.*, 2021] Jiequan Cui, Shu Liu, Liwei Wang, and Jiaya Jia. Learnable boundary guided adversarial training. In *Proceedings of the IEEE/CVF International Conference on Computer Vision*, pages 15721–15730, 2021.
- [Cuturi, 2013] Marco Cuturi. Sinkhorn distances: Light-speed computation of optimal transport. *Advances in neural information processing systems (NeurIPS)*, 26:2292–2300, 2013.
- [Deng *et al.*, 2009] Jia Deng, Wei Dong, Richard Socher, Li-Jia Li, Kai Li, and Li Fei-Fei. Imagenet: A large-scale hierarchical image database. In *2009 IEEE Conference on Computer Vision and Pattern Recognition*, pages 248–255, 2009.
- [Deng *et al.*, 2020] Yao Deng, Xi Zheng, Tianyi Zhang, Chen Chen, Guannan Lou, and Miryung Kim. An analysis of adversarial attacks and defenses on autonomous driving models. In *2020 IEEE International Conference on Pervasive Computing and Communications (PerCom)*, pages 1–10. IEEE, 2020.
- [Dong *et al.*, 2018] Yinpeng Dong, Fangzhou Liao, Tianyu Pang, Hang Su, Jun Zhu, Xiaolin Hu, and Jianguo Li. Boosting adversarial attacks with momentum. In *Proceedings of the IEEE conference on computer vision and pattern recognition (CVPR)*, pages 9185–9193, 2018.
- [Guo *et al.*, 2019] Chuan Guo, Jacob Gardner, Yurong You, Andrew Gordon Wilson, and Kilian Weinberger. Simple black-box adversarial attacks. In *International Conference on Machine Learning (ICML)*, pages 2484–2493. PMLR, 2019.
- [He *et al.*, 2016a] Kaiming He, Xiangyu Zhang, Shaoqing Ren, and Jian Sun. Deep residual learning for image recognition. In *Proceedings of the IEEE conference on computer vision and pattern recognition*, pages 770–778, 2016.
- [He *et al.*, 2016b] Kaiming He, Xiangyu Zhang, Shaoqing Ren, and Jian Sun. Identity mappings in deep residual networks. In *European conference on computer vision*, pages 630–645. Springer, 2016.
- [Helgason, 2010] Sigurdur Helgason. *Integral geometry and Radon transforms*. Springer Science & Business Media, 2010.
- [Hoffman *et al.*, 2019] Judy Hoffman, Daniel A Roberts, and Sho Yaida. Robust learning with jacobian regularization. *arXiv preprint arXiv:1908.02729*, 2019.

- [Ian *et al.*, 2014] Goodfellow Ian, Shlens Jonathon, and Szegedy Christian. Explaining and harnessing adversarial examples. *arXiv preprint arXiv:1412.6572*, 2014.
- [Jakubovitz and Giryes, 2018] Daniel Jakubovitz and Raja Giryes. Improving dnn robustness to adversarial attacks using jacobian regularization. In *Proceedings of the European Conference on Computer Vision (ECCV)*, pages 514–529, 2018.
- [Kannan *et al.*, 2018] Harini Kannan, Alexey Kurakin, and Ian Goodfellow. Adversarial logit pairing. *arXiv preprint arXiv:1803.06373*, 2018.
- [Krizhevsky *et al.*, 2009] Alex Krizhevsky, Geoffrey Hinton, et al. Learning multiple layers of features from tiny images. Technical report, University of Toronto, Toronto, 2009.
- [Kurakin *et al.*, 2016] Alexey Kurakin, Ian Goodfellow, Samy Bengio, et al. Adversarial examples in the physical world, 2016.
- [Ma *et al.*, 2021] Xingjun Ma, Yuhao Niu, Lin Gu, Yisen Wang, Yitian Zhao, James Bailey, and Feng Lu. Understanding adversarial attacks on deep learning based medical image analysis systems. *Pattern Recognition*, 110:107332, 2021.
- [Madry *et al.*, 2018] Aleksander Madry, Aleksandar Makelov, Ludwig Schmidt, Dimitris Tsipras, and Adrian Vladu. Towards deep learning models resistant to adversarial attacks. *International Conference on Learning Representations (ICLR)*, 2018.
- [Meng *et al.*, 2019] Cheng Meng, Yuan Ke, Jingyi Zhang, Mengrui Zhang, Wenxuan Zhong, and Ping Ma. Large-scale optimal transport map estimation using projection pursuit. *Advances in Neural Information Processing Systems (NeurIPS)*, 2019.
- [Moosavi-Dezfooli *et al.*, 2016] Seyed-Mohsen Moosavi-Dezfooli, Alhussein Fawzi, and Pascal Frossard. Deep-fool: a simple and accurate method to fool deep neural networks. In *Proceedings of the IEEE conference on computer vision and pattern recognition*, pages 2574–2582, 2016.
- [Pang *et al.*, 2020] Tianyu Pang, Xiao Yang, Yinpeng Dong, Hang Su, and Jun Zhu. Bag of tricks for adversarial training. *arXiv preprint arXiv:2010.00467*, 2020.
- [Petrovich *et al.*, 2020] Mathis Petrovich, Chao Liang, Ryoma Sato, Yanbin Liu, Yao-Hung Hubert Tsai, Linchao Zhu, Yi Yang, Ruslan Salakhutdinov, and Makoto Yamada. Feature robust optimal transport for high-dimensional data. *arXiv preprint arXiv:2005.12123*, 2020.
- [Qian, 1999] Ning Qian. On the momentum term in gradient descent learning algorithms. *Neural networks*, 12(1):145–151, 1999.
- [Rice *et al.*, 2020] Leslie Rice, Eric Wong, and Zico Kolter. Overfitting in adversarially robust deep learning. In *International Conference on Machine Learning*, pages 8093–8104. PMLR, 2020.
- [Rony *et al.*, 2019] Jérôme Rony, Luiz G Hafemann, Luiz S Oliveira, Ismail Ben Ayed, Robert Sabourin, and Eric Granger. Decoupling direction and norm for efficient gradient-based l2 adversarial attacks and defenses. In *Proceedings of the IEEE/CVF Conference on Computer Vision and Pattern Recognition (CVPR)*, pages 4322–4330, 2019.
- [Shafahi *et al.*, 2019] Ali Shafahi, Mahyar Najibi, Amin Ghiasi, Zheng Xu, John Dickerson, Christoph Studer, Larry S Davis, Gavin Taylor, and Tom Goldstein. Adversarial training for free! *arXiv preprint arXiv:1904.12843*, 2019.
- [Vialard, 2019] François-Xavier Vialard. An elementary introduction to entropic regularization and proximal methods for numerical optimal transport. 2019.
- [Villani, 2008] Cédric Villani. *Optimal transport: old and new*, volume 338. Springer Science & Business Media, 2008.
- [Wu *et al.*, 2020] Dongxian Wu, Shu-Tao Xia, and Yisen Wang. Adversarial weight perturbation helps robust generalization. *Advances in Neural Information Processing Systems*, 33:2958–2969, 2020.
- [Zagoruyko and Komodakis, 2016] Sergey Zagoruyko and Nikos Komodakis. Wide residual networks. *arXiv preprint arXiv:1605.07146*, 2016.
- [Zhang and Wang, 2019] Haichao Zhang and Jianyu Wang. Defense against adversarial attacks using feature scattering-based adversarial training. *Advances in Neural Information Processing Systems (NeurIPS)*, 32:1831–1841, 2019.
- [Zhang *et al.*, 2019] Hongyang Zhang, Yaodong Yu, Jiantao Jiao, Eric Xing, Laurent El Ghaoui, and Michael Jordan. Theoretically principled trade-off between robustness and accuracy. In *International Conference on Machine Learning (ICML)*, pages 7472–7482. PMLR, 2019.
- [Zhang *et al.*, 2020] Jingfeng Zhang, Jianing Zhu, Gang Niu, Bo Han, Masashi Sugiyama, and Mohan Kankanhalli. Geometry-aware instance-reweighted adversarial training. *International Conference on Learning Representations (ICLR)*, 2020.

1 Threat Model and Adversarial Sample

In this section, we summarize essential terminologies of adversarial settings related to our work. We first define a threat model, which consists of a set of assumptions about the adversary. Then, we describe the generation mechanism of adversarial samples in AT frameworks for the threat model defending against adversarial attacks.

1.1 Threat Model

Adversarial perturbation was firstly discovered by Christian *et al.*, and it instantly strikes an array of studies in both adversarial attack and adversarial robustness. Carlini *et al.* specifies a threat model for evaluating a defense method including a set of assumptions about the adversary’s goals, capabilities, and knowledge, which are briefly delineated as follows:

- Adversary’s goals could be either simply deceiving a model to make the wrong prediction to any classes from a perturbed input or making the model misclassify a specific class to an intended class. They are known as *untargeted* and *targeted* modes, respectively.
- Adversary’s capabilities define reasonable constraints imposed on the attackers. For instance, a L_p certified robust model is determined with the worst-case loss function \mathcal{L} for a given perturbation budget ϵ :

$$\mathbb{E}_{(x,y)\sim\mathcal{D}} \left[\max_{\tilde{x}\in B_p(x,\epsilon)} \mathcal{L}(f(\tilde{x}), y) \right], \quad (15)$$

where $B_p(x, \epsilon) = \{u \in \mathbb{R}^Z : \|u - x\|_p \leq \epsilon\}$.

- Adversary’s knowledge indicates what knowledge of the threat model that an attacker is assumed to have. Typically, *white-box* and *black-box* attacks are two most popular scenarios studied. The white-box settings assume that attackers have full knowledge of the model’s parameters and its defensive scheme. In contrast, the black-box settings have varying degrees of access to the model’s parameter or the defense.

Bearing these assumptions about the adversary, we describe how a defense model generates adversarial samples for its training in the following section.

1.2 Adversarial Sample in AT

Among multiple attempts to defend against adversarial perturbed samples, adversarial training (AT) is known as the most successful defense method. In fact, AT is an data-augmenting training method that originates from the work of [Ian *et al.*, 2014], where crafted adversarial samples are created by the fast gradient sign method (FGSM), and mixed into the mini-batch training data. Subsequently, a wide range of studies focus on developing powerful attacks [Kurakin *et al.*, 2016; Dong *et al.*, 2018; Carlini and Wagner, 2017;

Croce and Hein, 2020a]. Meanwhile, in the opposite direction to the adversarial attack, there are also several attempts to resist against adversarial examples [Kannan *et al.*, 2018; Zhang and Wang, 2019; Shafahi *et al.*, 2019]. In general, a defense model is optimized by solving a minimax problem:

$$\min_{\theta} \left[\max_{\tilde{x}\in B_p(x,\epsilon)} \mathcal{L}_{\mathcal{X}\mathcal{E}}(\tilde{x}, y; \theta) \right], \quad (16)$$

where the inner maximization tries to successfully create perturbation samples subjected to an ϵ -radius ball B around the clean sample x in L_p space. The outer minimization tries to adjust the model’s parameters to minimize the loss caused by the inner attacks. Among existing defensive AT, PGD-AT [Madry *et al.*, 2018] becomes the most popular one, in which the inner maximization is approximated by the multi-step projected gradient (PGD) method:

$$\tilde{x}_{t+1} = \Pi_x^\epsilon(\tilde{x}_t + \eta \cdot \text{sgn}(\nabla_{\tilde{x}} \mathcal{L}(\tilde{x}_t, y))), \quad (17)$$

where Π_x^ϵ is an operator that projects its input into the feasible region $B_\infty(x, \epsilon)$, and $\eta \in \mathbb{R}$ is called step size. The loss function in Eq. 17 can be modulated to derive different variants of generation mechanism for adversarial samples in AT. For example, Zhang *et al.* [Zhang *et al.*, 2019] utilizes the loss between the likelihood of clean and adversarial samples for updating the adversarial samples. In our work, we use Eq. 17 as our generation mechanism for our AT framework.

1.3 Adversarial attacks

For the *white-box* attacks, we deploy the followings in our experiment:

- **FGSM** [Ian *et al.*, 2014]: Adversarial samples are generated under the L_∞ norm as follows:

$$x^{adv} = x + \epsilon \cdot \text{sgn}(\nabla_x \mathcal{L}_{\mathcal{X}\mathcal{E}}(x, y)). \quad (18)$$

- **PGD** [Madry *et al.*, 2018]: Its initial point x_0^{adv} is uniformly sampled from the neighbor around x .
- **MIM** [Dong *et al.*, 2018]: It is the integration of BIM and a momentum with decay factor μ as:

$$g_{t+1} = \mu \cdot g_t + \frac{\nabla_x \mathcal{L}_{\mathcal{X}\mathcal{E}}(x_t^{adv}, y)}{\|\nabla_x \mathcal{L}_{\mathcal{X}\mathcal{E}}(x_t^{adv}, y)\|_1}, \quad (19)$$

and the adversarial samples are then updated by:

$$x_{t+1}^{adv} = \text{clip}_{x,\epsilon}(x_t^{adv} + \eta \cdot \text{sgn}(g_{t+1})), \quad (20)$$

- **C&W** [Carlini and Wagner, 2017]: Adversarial samples are generated under L_2 norm by solving:

$$x^{adv} = \arg \min_{x'} [c \cdot \max(f(x')_y - \max_{i \neq y} f(x')_i, 0) + \|x' - x\|_2], \quad (21)$$

where c is a variable that found by binary search.

- **FAB** [Croce and Hein, 2020a]: It iteratively generates adversarial samples lie on the decision boundaries of a classifier with minimal perturbation. We implement both targeted and untargeted FAB attacks.

Meanwhile, we utilize the following *black-box* attacks:

- **Square** [Andriushchenko *et al.*, 2020]. It is an efficient random search-based adversarial attack that generates L_∞ adversarial sample by continuously adding small windows of perturbation h to the clean image, which has size of $w \times w \times c$ until success:

$$x_{t+1}^{adv} = x_t^{adv} + \delta, \delta \sim P(\epsilon, h_{t+1}, w, c, x_t^{adv}, x), \quad (22)$$

where P is the uniform distribution with values are in $\{-2\epsilon, 2\epsilon\}$.

- **SimBA** [Guo *et al.*, 2019]. This approach iteratively chooses a random vector q from an orthonormal input space Q and adds this vector to the clean image as follows:

$$x_{t+1}^{adv} = x_t^{adv} + \alpha \cdot q, \alpha \in \{\epsilon, -\epsilon\}. \quad (23)$$

2 Detailed Implementation of OTJR

Listing 1: OTJR Python Code Implementation

```
import torch
from torch.autograd import grad
"""
Arguments:
    x: (batch_size, 3, H, W)
    lb: (batch_size, )
    src, tgt: (batch_size, C)
    K: number of projection
"""
# generate random projections
projs = torch.randn(size=(dim, K))
l2 = projs.pow(2).sum(0, True).pow(0.5)
# normalize projections
projs = projs.div(l2)
# project 'src' and 'tgt' distributions
src_p = src.matmul(projs).transpose(0,1)
tgt_p = tgt.matmul(projs).transpose(0,1)
# ascending sort
tgt_sort, _ = torch.sort(tgt_p,1)
src_rank = torch.argsort(
    torch.argsort(src_p), 1)
# tau_1^{-1} o tau_2 in Eqn.10
tgt2src = torch.gather(input=tgt_sort,
    dim=1, index=src_rank)
# movement
src_move = tgt2src - src_p
sw = src_move.pow(2).sum() # Eqn.9
m = torch.zeros_like(src)
for i in range(K):
    m += torch.outer(torch.squeeze(
        src_move[i]), projs[:,i]) # Eqn. 10
l2 = m.pow(2).sum(1, True).pow(0.5)
delta = m.div(l2) # Eqn. 11
J = grad(x.reshape(-1),
    delta.reshape(-1),
    retain_graph=True,
    create_graph=True
    ).norm().pow(2) # Eqn. 12
```

We include the pseudo-code as an example, implemented with PyTorch, of how the SW distance and optimal Jacobian regularization are calculated (List 1). We use ψ function as the square of l_2 loss. Note that $\psi(\tau_1 \circ \mathcal{R}_{\hat{v}_k} \mu, \tau_2 \circ \mathcal{R}_{\hat{v}_k} \nu) = \psi(\tau_1^{-1} \circ \tau_2 \circ \mathcal{R}_{\hat{v}_k} \nu, \mathcal{R}_{\hat{v}_k} \mu)$, since l_2 loss is applied in element-wise, and τ_1^{-1} now becomes the rank of the values in $\mathcal{R}_{\hat{v}_k} \mu$.

3 Further Empirical Analyses

In this section, we conduct intensive experiments on various AT methods.

3.1 Smaller backbone experiment

Similar to our main experiment, we provide a comparison between our OTJR training framework with different defense methods in Table 9 with a smaller backbone - WRN28. Hyper-parameters are kept the same as we used. We note that our proposed framework achieves significant improvements across various while-box and black-box attacks.

3.2 Sanity Tests

Gradient obfuscation is observed when a defense method is designed such that its gradients are not useful for generating adversarial samples [Athalye *et al.*, 2018]. However, the method designed in that manner can be an incomplete defense to adversarial examples [Athalye *et al.*, 2018]. We follow the recommendations in [Carlini *et al.*, 2019], and show that our proposed OTJR does not rely on gradient obfuscation. Particularly, as shown in Table 10, iterative attacks are strictly more powerful than single-step attacks, whereas when increasing perturbation budget ϵ can also raise attack successful rate. Finally, the PGD attack reaches 100% successful rate when $\epsilon = 128/255$.

3.3 Training Time

Table 11 indicates the average training time per epoch of all AT methods on our machine architecture using WRN34 model on CIFAR-100 dataset. While the SAT algorithm shows a decent training time per epoch, the total number of training epochs it requires for convergence can be quadruple compared to others when it is trained on large scale datasets, *e.g.*, CIFAR-100. As we can observe, while our method can show a significant improvement over previous SOTA frameworks, its computation time in the training phase is acceptable.

3.4 Progression of input derivatives

Table 12 shows the progression of input derivatives after different PGD white-box attack iterations. We note that the perturbation noises created by the output loss derivatives increase when more attack iterations are applied. Nevertheless, our proposed framework maintains the smallest silence throughout the iterations. This experiment further proves our OTJR’s robustness performance.

Dataset	Defense	Clean	PGD ²⁰	PGD ¹⁰⁰	L_2 -PGD	MIM	FGSM	CW	FAB	Square	SimBa	AutoAtt
CIFAR-10	TRADES	84.52	54.06	53.85	61.07	54.10	60.27	53.08	53.43	62.35	70.84	51.91
	ALP	85.90	47.31	46.77	55.98	47.16	57.96	47.73	53.35	59.43	68.82	46.46
	PGD-AT	86.39	46.69	46.22	56.33	46.61	56.36	47.44	48.12	58.96	68.40	45.98
	SAT	82.85	53.34	53.06	60.49	53.34	59.57	51.69	52.22	60.73	69.79	50.50
	OTJR (Ours)	83.63	55.25	54.87	64.16	55.08	60.48	53.41	53.58	62.61	71.73	52.03
CIFAR-100	TRADES	57.52	30.27	30.07	36.10	30.19	32.78	28.21	27.47	33.41	44.34	26.46
	ALP	61.08	25.83	25.40	33.55	25.74	30.97	25.59	25.14	32.57	43.78	23.89
	PGD-AT	59.73	23.45	23.11	31.08	23.47	28.92	24.62	23.86	31.07	41.27	22.57
	SAT	53.27	26.82	26.63	31.99	26.67	30.96	25.30	26.26	30.83	40.45	24.31
	OTJR (Ours)	57.82	31.84	31.71	42.87	31.84	34.08	29.65	28.25	36.06	49.44	27.78

Table 9: **Classification accuracy (%) under white-box, black-box attacks and AutoAttack.** Different defense methods trained on CIFAR-10 and CIFAR-100 datasets using WRN28, where subscript indicates training epochs. Best results are in **bold**.

Number of step					
Clean	1	10	20	40	50
84.91	79.45	56.05	55.07	54.72	54.72
Perturbation budget ϵ w/ PGD-20					
Clean	8/255	16/255	24/255	64/255	128/255
84.91	55.07	23.66	9.18	0.57	0.00

Table 10: **Basic sanity tests for our OTJR method with white-box PGD attack.**

Method	Time(mins)	Method	Time(mins)
$\mathcal{X}\mathcal{E}$	1.27	PGD-AT	13.67
ALP	14.67	TRADES	18.15
SAT	13.97	OTJR (Ours)	18.68

Table 11: **Training time per epoch** of AT methods. Even though our method’s training time/epoch is slightly slower than the SAT’s as the additional Jacobian regularization, it can achieve faster convergence on large-scale datasets.

3.5 Activation Magnitude

Fig. 8 illustrates activation magnitudes at the penultimate layer of WRN34 for all AT frameworks. While AT methods can adjust the adversarial magnitudes closed to their clean, their overall magnitudes keep high, especially PGD-AT. By balancing the input Jacobian matrix and output distributions, our proposed method can reduce the model’s surprises when encountering perturbed samples.

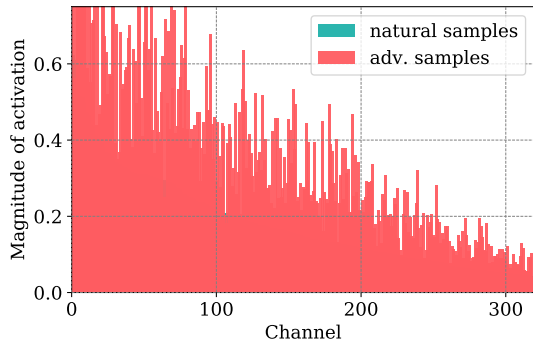
4 Broader Impact

Using machine learning models in a practical system requires sufficient accuracy and robustness when encountering different environment scenarios. Our primary aim behind this work is to develop a training framework that can enhance a DNN model’s robustness under a wide range of adversarial attacks, including white-box and black-box settings. To this end, we propose our novel OTJR framework that can optimize the conventional Jacobian regularization and align the output distributions. We believe our work makes essential progress in combining both adversarial training and input-output Jacobian regularization, which have been so far overlooked, for

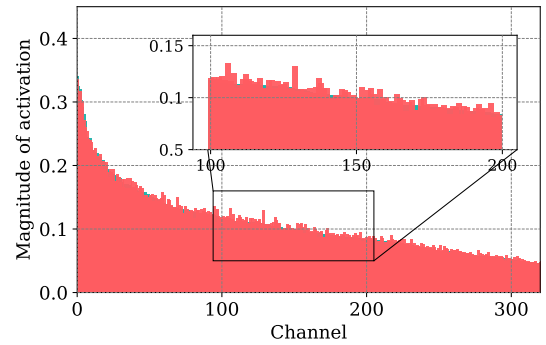
achieving a more reliable model.

<i>Method</i>	$\mathbb{E}(\ \nabla_x \mathcal{L}\ _1)$					
	<i>Clean</i> ($\times e^{-4}$)	<i>PGD</i> ¹ ($\times e^{-4}$)	<i>PGD</i> ⁵ ($\times e^{-4}$)	<i>PGD</i> ¹⁰ ($\times e^{-4}$)	<i>PGD</i> ¹⁵ ($\times e^{-4}$)	<i>PGD</i> ²⁰ ($\times e^{-4}$)
$\mathcal{X}\mathcal{E}$	854	5492	4894	4852	4975	4900
Random JR	105	149	272	335	360	370
PGD	158	232	420	520	568	586
ALP	118	161	249	298	322	332
TRADES	45	53	73	84	89	90
SAT	48	54	65	75	81	84
OTJR (Ours)	43	48	61	70	73	75

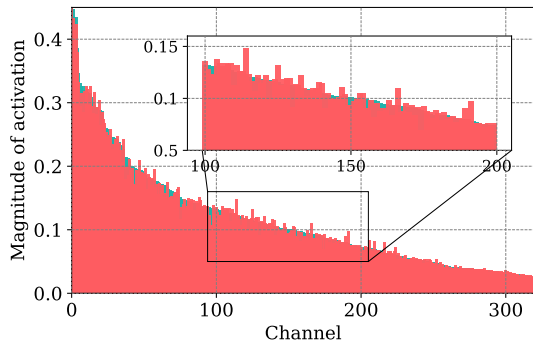
Table 12: **Average derivative of $\mathcal{X}\mathcal{E}$ loss w.r.t** input x at the pixel level after various PGD iterations. The lower the derivative is, the less perturbed the adversarial samples are when the model is abused. Best results are in **bold**.



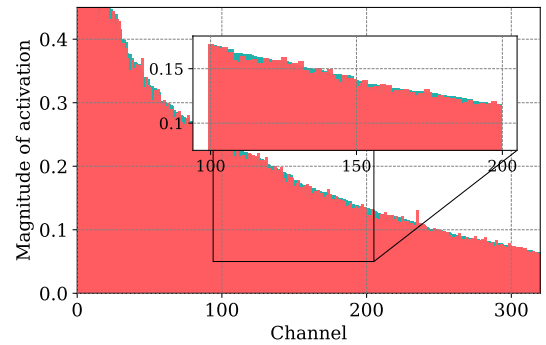
(a) $\mathcal{X}\mathcal{E}$



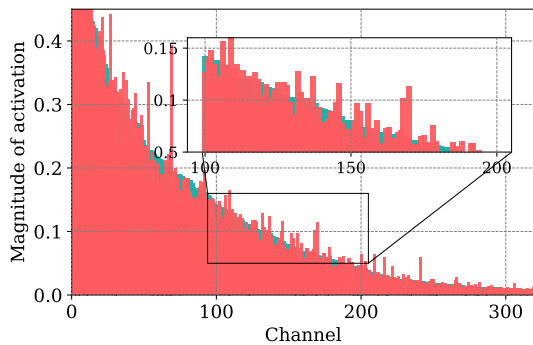
(b) TRADES



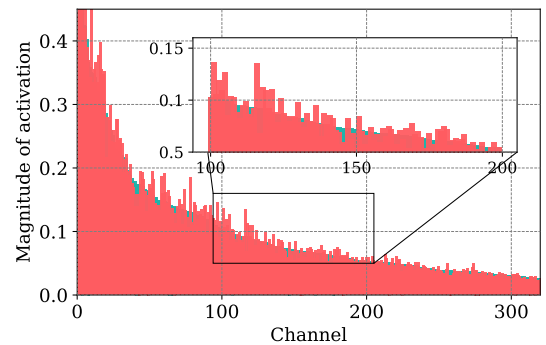
(c) ALP



(d) PGD-AT



(e) SAT



(f) OTJR (*Ours*)

Figure 8: **Magnitude of activation** at the penultimate layer for models trained with different defense methods. Our OTJR can regulate adversarial samples' magnitudes similar to clean samples' while well suppressing both of them.

5 Gallery of Cross Decision Cells

This section provides more illustrations about the benefit of optimal Jacobian regularization in increasing decision boundaries for a defense model.

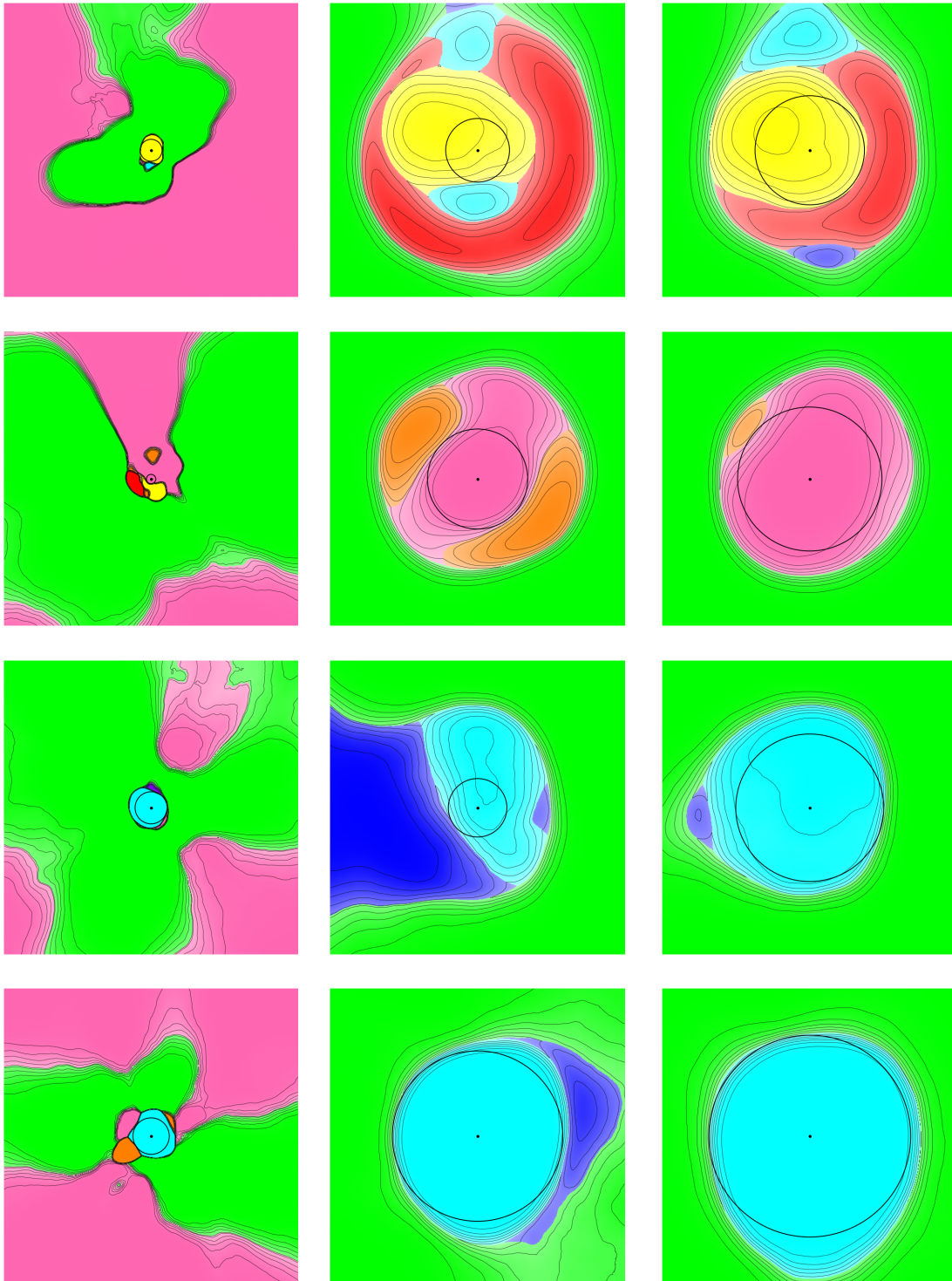


Figure 9: **Cross sections of decision boundaries in the input space. Left column:** Model trained without regularization. **Middle column:** Model train with Jacobian regularization having random projection. **Right column:** Model trained with Jacobian regularization having informative projections. Our optimal JR benefits from the informative directions obtained by SW distance, and thus helps the model to regularize these sensitive direction of clean samples and produce larger decision cells